

Design-oriented Modeling of 28 nm FDSOI CMOS Technology down to 4.2 K for Quantum Computing

Arnout Beckers[†], Farzan Jazaeri[†], Heorhii Bohuslavskyi[‡], Louis Hutin[‡], Silvano De Franceschi[‡], and ChristianENZ[†]

[†]Integrated Circuits Laboratory (ICLAB), Ecole Polytechnique Fédérale de Lausanne (EPFL), Switzerland,

[‡]CEA-Léti, Grenoble, France

arnout.beckers@epfl.ch

Abstract—In this paper a commercial 28-nm FDSOI CMOS technology is characterized and modeled from room temperature down to 4.2 K. Here we explain the influence of incomplete ionization and interface traps on this technology starting from the fundamental device physics. We then illustrate how these phenomena can be accounted for in circuit device-models. We find that the design-oriented simplified EKV model can accurately predict the impact of the temperature reduction on the transfer characteristics, back-gate sensitivity, and transconductance efficiency. The presented results aim at extending industry-standard compact models to cryogenic temperatures for the design of cryo-CMOS circuits implemented in a 28 nm FDSOI technology.

I. INTRODUCTION

Quantum computing can reshape many fields by providing the computing power to solve exponentially-growing problems. To reach this computing power, an important challenge today is the scale-up to larger qubit numbers [1], [2]. Each additional qubit adds to the complexity of the room-temperature control-equipment, introducing more interconnections, wiring capacitance and thermal-noise pickup. Implementing the control equipment in miniaturized cryo-CMOS represents an interesting solution for scalability and fast qubit-information processing. Digital, analog and RF circuits are then required to operate down to deep-cryogenic temperatures. In this context, silicon-on-insulator technology provides an excellent platform to create a complete, scalable quantum computing system [3], [4]. CMOS-compatible spin qubits have been developed in a FDSOI nanowire technology [5], [6], and can be co-integrated with the required qubit-control circuits designed in a FDSOI CMOS process. Increased digital/analog performances down to 4.2 K have been reported for advanced FDSOI CMOS technologies [7], [8]. The suitability of the 28 nm node for qubit-control electronics has been reported in [7]. Furthermore, the FDSOI back-gate offers a versatile tool to control the power consumption close to the qubits [7], which may become essential to keep decoherence at bay in co-integrated quantum-classical circuits. Due to a strong reduction of the cooling power at millikelvin temperatures, the control circuits are envisioned to operate at 4.2 K or higher—and eventually the qubits as well [2]. However, designing the cryo-CMOS qubit-control circuits—while meeting a stringent speed-power trade-

TABLE I
INVESTIGATED DEVICES (28-NM FDSOI CMOS PROCESS)

Symbol	Type	W/L
●	<i>n</i> MOS	1 μm / 1 μm
▲	<i>p</i> MOS	1 μm / 1 μm
▼	<i>n</i> MOS	1 μm / 28 nm
■	<i>n</i> MOS	210 nm / 28 nm
◆	<i>n</i> MOS	80 nm / 28 nm

off—is not an easy task, since cryo-CMOS device models are currently lacking in circuit-simulators. In order to keep pace with the rapid qubit-developments, device models remaining physically accurate down to 4.2 K are urgently required. To this purpose, important physical phenomena at deep-cryogenic temperatures, i.e. interface trapping and incomplete ionization, need to be included. Here, after a brief discussion of the measurement results down to 4.2 K, the temperature-trends of the main technological parameters are investigated (Sec. II). To explain some of these trends, we examine the temperature dependencies of interface trapping and incomplete ionization in the device physics of this technology (Sec. III). It will be evidenced that these phenomena can respectively alter the slope factor and the threshold voltage. As we will demonstrate, adjusting the corresponding model parameters in the design-oriented simplified EKV model, allows to model the DC cryogenic device-performance down to 4.2 K, including the effect of the back-gate (Sec. IV). These results pave the way towards the extension of industry-standard compact models down to the deep-cryogenic temperature regime [9], [10]. This will allow to explore optimal cryo-CMOS circuit designs for multiple applications, in particular qubit-control systems.

II. MEASUREMENTS AND CHARACTERIZATION

The set of devices under investigation, fabricated in a commercial 28 nm FDSOI CMOS process, is listed in Table I. Details on the fabrication procedure can be found in [7]. A schematic cross-section of the FDSOI *n*MOS transistor is drawn in Fig. 1a. The transfer characteristics were measured in the linear ($V_{DS} = 50$ mV) and saturation operational regimes ($V_{DS} = 0.9$ V) at different temperatures [7]. The back-gate voltage (V_{back}) is swept from -0.9 V to 0.9 V. Figs. 1b-f show the transfer characteristics in saturation at $V_{back} = 0$ V. The strong improvement of the *SS* with decreasing temperature is clear for all devices in Fig. 1. However, note

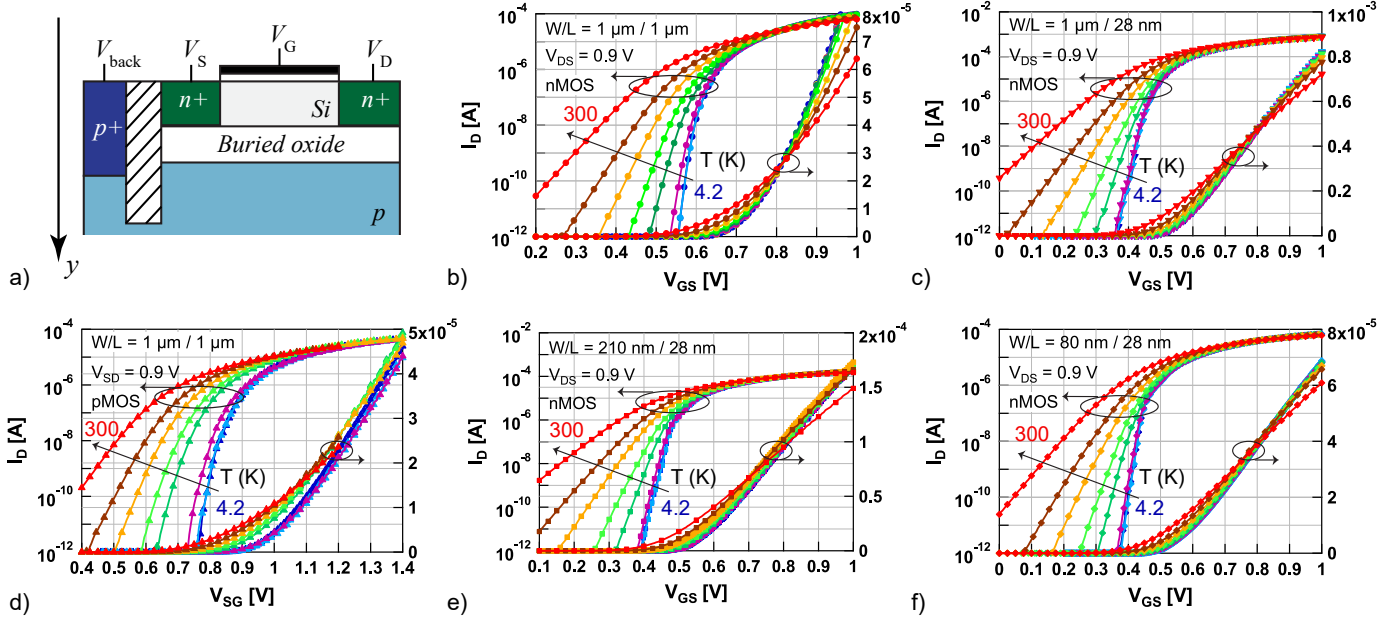


Fig. 1. a) Schematic cross-section of a nMOS device fabricated in a 28 nm FDSOI CMOS process [7], b)-f) Transfer characteristics measured in saturation ($|V_{DS}| = 0.9 \text{ V}$) with $V_{back} = 0 \text{ V}$, at 300, 210, 160, 110, 77, 36, 10, and 4.2 K for b) nMOS $W/L = 1 \mu\text{m} / 1 \mu\text{m}$, c) nMOS $W/L = 1 \mu\text{m} / 28 \text{ nm}$, d) pMOS $W/L = 1 \mu\text{m} / 1 \mu\text{m}$, e) nMOS $W/L = 210 \text{ nm} / 28 \text{ nm}$, and f) nMOS $W/L = 80 \text{ nm} / 28 \text{ nm}$. The EOT for nMOS is 1.55 nm, and for pMOS 1.7 nm. The gate-source voltage is increased with a step size of $|V_{GS}| = 5 \text{ mV}$. Colors indicate the temperature, and markers the device according to Table I.

that the improvement from 36 K down to 4.2 K is marginal, especially for the short devices. Based on the measurements in Fig. 1, the following technological parameters have been extracted (Fig. 2): the subthreshold swing (SS), slope factor (n), threshold voltage (V_{th}), transconductance in linear and saturation ($G_{m,lin}$, $G_{m,sat}$), and the on-state current (I_{on}). As illustrated in Fig. 2a, for temperatures below $\approx 160 \text{ K}$, the extracted average SS -values show an increasing offset, ΔSS , from the thermal limit, $U_T \ln 10$, with $U_T \triangleq kT/q$ the thermal voltage. ΔSS reaches around 10 mV/dec at 4.2 K for long nMOS, since $U_T \ln 10$ predicts $\approx 0.8 \text{ mV/dec}$. The necessary slope factors to reach such high SS are extracted in Fig. 2b using $n = SS / (U_T \ln 10)$. From this figure, a hyperbolic temperature-dependency of n is evident, which is not strongly dependent on geometry at cryogenic temperatures. The data points below 77 K in Fig. 2a cannot be explained by $n_0 U_T \ln 10$ with a slope-factor n_0 limited by 2, according to $n_0 = 1 + C_{dep} / C_{ox}$, where C_{dep} is the depletion capacitance and C_{ox} the oxide capacitance. Moreover, including the interface-trap capacitance, $C_{it} = qN_{it}$, i.e. $n_0 = 1 + (C_{dep} + C_{it}) / C_{ox}$ with N_{it} the density-of-interface-traps per unit area, would lead to very high extracted values for N_{it} in the order of 10^{13} cm^{-2} at 4.2 K [11]–[13]. However, it should be emphasized that in this n_0 -formula the temperature-dependent occupation of interface-traps is not taken into account. This will be further investigated in Sec. III. The shift in threshold voltage at 4.2 K with respect to room temperature increases in the order of 0.1–0.3 V (Fig. 2c). Note that the largest V_{th} -increase is observed for pMOS, similarly to a 28-nm bulk process [14]. Furthermore, the maximum $G_{m,sat}$ and $G_{m,lin}$

(Figs. 2d-e) improve down to 4.2 K, e.g. respectively $\times 3.4$ (linear) and $\times 1.8$ (saturation) for nMOS $W/L = 1 \mu\text{m} / 1 \mu\text{m}$. In Fig. 2f, I_{on} is extracted at $|V_{GS}| = 1 \text{ V}$. Note that the actual trend of I_{on} with temperature is strongly dependent on the bias and the device-type. At a standard supply-voltage of 1 V, the on-state current increases with decreasing temperature for long nMOS (Fig. 1b), while it decreases for pMOS (Fig. 1d). The drain-induced barrier-lowering (DIBL) is approximately zero for the long devices. For the short devices, small improvements have been extracted down to 4.2 K, but the short-channel effect remains largely temperature-independent, e.g. decreasing from 0.07 V/V (300 K) to 0.068 V/V (4.2 K) for nMOS $W/L = 80 \text{ nm} / 28 \text{ nm}$, and from 0.065 V/V (300 K) to 0.059 V/V (4.2 K) for nMOS $W/L = 210 \text{ nm} / 28 \text{ nm}$ (extracted at $I_D = 10^{-8} \text{ A}$).

III. DEVICE PHYSICS

The improvements of (SS , $G_{m,sat}$, $G_{m,lin}$) and the increase in V_{th} follow directly from the temperature-scaling of the Fermi-Dirac distribution function, $f(E)$. As illustrated in Fig. 3a, at 4.2 K $f(E)$ is almost a step function. Therefore, the conduction band needs to be bent further downward to create sufficient overlap with the conduction-band density-of-states to reach inversion, increasing V_{th} . Note that the subthreshold region happens only when E_F lies within $\approx 3U_T$ of E_c . However, as indicated by ΔSS in the previous section, the turn-on rate predicted in this way is too steep. In what follows, we investigate the impact of incomplete ionization/freez-out and interface trapping to explain this observation. Both phenomena are modeled by the Fermi-Dirac distribution as

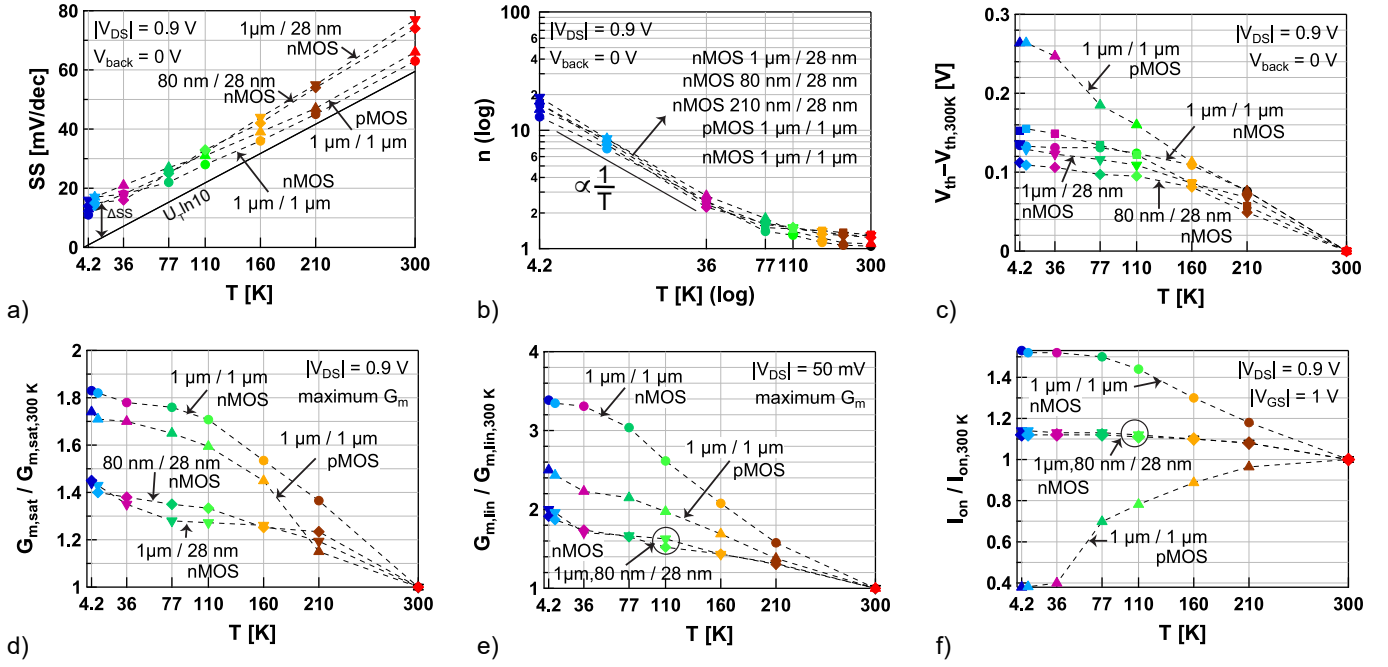


Fig. 2. Technological parameter extraction at 300, 210, 160, 110, 77, 36, 10, and 4.2 K, a) Subthreshold swing, modeled for long-channel devices by $SS = n_0 U_T \ln 10 + \Delta SS$, with $\Delta SS \propto N_{it}$ [15], [16], b) Slope factor in log-log scale highlighting its hyperbolic temperature dependency, c) Threshold-voltage shift with respect to 300 K, d-e) Maximum transconductances in saturation and linear regions of operation, normalized to 300 K, f) On-state current normalized to 300 K. Colors indicate the temperature, and markers the device according to Table I.

well, i.e. respectively $f(E_A)$ (for p -type doping) and $f(E_t)$, where E_A and E_t are the acceptor and trap energy levels. This is qualitatively shown in Fig.3a. In case the Si-channel (Fig. 1a) is truly undoped, incomplete ionization should not be considered. However, if there is a certain background doping, e.g. p -type $N_A = 10^{15} \text{ cm}^{-3}$, these impurities can be frozen out in the flatband condition at 4.2 K. As shown in Fig.3a, the calculated E_F -position for low-doped channel at 4.2 K lies under E_A , leading to freeze-out ($f(E_A) \ll 1$). Nonetheless, these impurities will become quickly ionized due to field-assisted ionization [17], when E_A bends under E_F near the surface of the front-gate. In the subthreshold region, when $E_F \approx E_c - 3U_T$, complete ionization can be assumed. Therefore, incomplete ionization cannot lead to the subthreshold-swing degradation observed in the previous section. Note, however, that for non-zero doping concentrations incomplete ionization can yield a small change in the threshold voltage, due to a modification of the charge-neutrality and the resulting E_F -position [16]. Fig.3a highlights that the temperature-dependency of interface-trap occupation, $f(E_t)$, may influence the turn-on rate of the device down to 4.2 K. Similarly to the derivation for bulk MOSFET presented in [16], by including $f(E_t)$ the temperature dependency of $n \propto 1/U_T$ for long (Figs.3b-c) and short devices (Fig.3d). This gives $SS = n(T)U_T \ln 10 = n_0 U_T \ln 10 + \Delta SS$, where n_0 is the slope factor without interface traps, and ΔSS the subthreshold-swing offset as observed in the previous section. ΔSS is given by $(qN_{it}/C_{ox}) \ln 10 [g_t/(1 + g_t)^2]$ with N_{it} the density-of-interface-traps and g_t the trap degeneracy factor.

Note that in this model, N_{it} does not become multiplied with U_T , resulting in reasonable extracted values for N_{it} at 4.2 K ($\approx 10^{11}$ - 10^{12} cm^{-2}) lower than [12], [13]. The ΔSS -offset starts to increase below ≈ 160 K since the subthreshold region happens when E_F lies closer to E_c , where N_{it} is observed to be higher already at 300 K (Fig.3a). From this section, we conclude that interface trapping strongly degrades the SS through the hyperbolic temperature-dependency of n , and incomplete ionization slightly alters the V_{th} -increase for non-zero doping concentrations. These two parameters, n and V_{th} , can be modified accordingly in design-oriented models to predict deep-cryogenic operation. In the next section we demonstrate this relying on the simplified EKV model.

IV. DESIGN-ORIENTED MODELING

The design-oriented simplified EKV model is described in detail in [18]. The suitability of this model for FDSOI processes has been assessed at room temperature [19]. Using this model, the effects of the temperature reduction down to 4.2 K on the transfer characteristics, the back-gate sensitivity, and the transconductance efficiency are modeled. The model accurately predicts the transfer characteristics down to 4.2 K for the interface-trapping phenomenon. The V_{T0} model parameter captures the change in the threshold voltage due to Fermi-Dirac scaling and incomplete ionization. Note that the used values for n and V_{T0} correspond to the extracted values in Fig. 2b and 2c. Furthermore, as illustrated in Fig. 3e, changing the V_{T0} model parameter allows to capture the effect of the

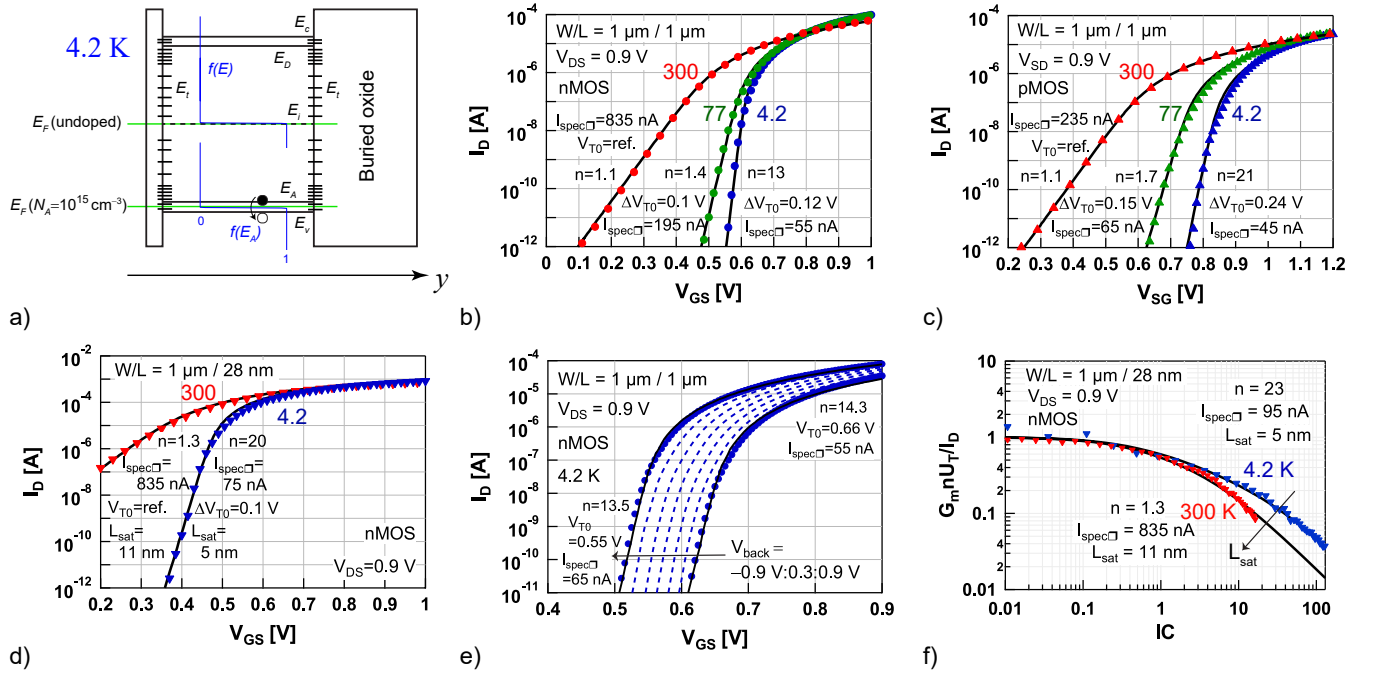


Fig. 3. Band diagram along the y -direction in Fig. 1a. The position of the Fermi-level, E_F , is calculated at 4.2 K in the case of undoped and low-doped channel, including incomplete ionization and bandgap widening at 4.2 K. The simulated Fermi-Dirac distribution at 4.2 K is plotted for both cases. The temperature-dependent occupation of the interface traps, $f(E_t)$, can degrade the subthreshold swing. Due to band bending of E_A under E_F at the front-gate, frozen-out impurities under the surface become completely ionized ($f(E_A) = 1$), long before subthreshold is reached ($E_F \approx E_c - 3U_T$) due to field-assisted ionization. b)-e) Simplified EKV (solid lines) for b) nMOS $W/L = 1 \mu\text{m} / 1 \mu\text{m}$, c) pMOS $W/L = 1 \mu\text{m} / 1 \mu\text{m}$, and d) nMOS $W/L = 1 \mu\text{m} / 28 \text{ nm}$ at 300, 77, and 4.2 K (markers) for $V_{back} = 0 \text{ V}$. The model parameters, n , V_{T0} (threshold voltage), $I_{spec\Box}$ (specific-current-per-square), and L_{sat} (saturation length), are shown. e) Back-gate sensitivity at 4.2 K modeled with simplified EKV. The model is shown for $V_{back} = -0.9 \text{ V}$ and 0.9 V with solid lines. Markers and dashed lines indicate measurements at 4.2 K, f) Normalized transconductance efficiency versus the inversion coefficient, IC , at 300 and 4.2 K.

back-gate also at 4.2 K [19]. A small adjustment of the slope factor is necessary as well, to account for the change in SS induced by the back-gate. Fig. 3f verifies that the G_m/I_D design-methodology remains valid for a 28 nm FDSOI technology down to 4.2 K. The normalized transconductance efficiency, $G_m n U_T / I_D$, is plotted versus the inversion coefficient $IC \triangleq I_{D,sat} / I_{spec}$, with $I_{spec} = I_{spec\Box} W/L = 2(W/L)n\mu C_{ox} U_T^2$. The specific-current-per-square, $I_{spec\Box}$, decreases over one order of magnitude from room temperature down to 4.2 K. For the short-channel device, the additional L_{sat} -parameter, which denotes the length of the channel in full velocity saturation, decreases down to 4.2 K due to a reduced phonon scattering.

V. CONCLUSION

In this work, the DC operation of a 28 nm FDSOI technology is modeled down to 4.2 K by means of the simplified EKV model. A study of the device physics is first performed including the temperature dependencies of interface trapping and incomplete ionization. We find that the Fermi-Dirac temperature dependency of interface-trap occupation explains the large degradation of the subthreshold swing at 4.2 K. In case impurities are present, freeze-out is of minor importance for device operation thanks to field-assisted ionization. These results bring us one step closer to the realization of large-scale silicon-based quantum computing systems.

REFERENCES

- [1] C. G. Almudever, L. Lao *et al.*, "The engineering challenges in quantum computing," in *Design, Automation Test in Europe Conference Exhibition (DATE)*, 2017, March 2017, pp. 836–845.
- [2] L. M. K. Vandersypen, H. Bluhm *et al.*, "Interfacing spin qubits in quantum dots and donors: hot, dense, and coherent," *npj Quantum Information*, vol. 3, no. 1, p. 34, Sep. 2017.
- [3] S. R. Ekanayake, T. Lehmann *et al.*, "Characterization of SOS-CMOS FETs at Low Temperatures for the Design of Integrated Circuits for Quantum Bit Control and Readout," *IEEE Transactions on Electron Devices*, vol. 57, no. 2, pp. 539–547, Feb. 2010.
- [4] S. D. Franceschi, L. Hutin *et al.*, "SOI technology for quantum information processing," in *2016 IEEE International Electron Devices Meeting (IEDM)*, Dec. 2016, pp. 13.4.1–13.4.4.
- [5] R. Maurand, X. Jehl *et al.*, "A CMOS silicon spin qubit," *Nature Communications*, vol. 7, p. 13575, Nov. 2016.
- [6] L. Hutin, R. Maurand *et al.*, "Si CMOS platform for quantum information processing," in *2016 IEEE Symposium on VLSI Technology*, June 2016, pp. 1–2.
- [7] H. Bohuslavskyi, S. Barraud *et al.*, "28nm Fully-depleted SOI technology: Cryogenic control electronics for quantum computing," in *2017 Silicon Nanoelectronics Workshop (SNW)*, 2017, pp. 143–144.
- [8] F. Balestra and G. Ghibaudo, "Physics and performance of nanoscale semiconductor devices at cryogenic temperatures," *Semiconductor Science and Technology*, vol. 32, no. 2, p. 023002, 2017.
- [9] T. Poiroux, O. Rozeau *et al.*, "Leti-UTSOI2.1: A Compact Model for UTBB-FDSOI Technologies Part II: DC and AC Model Description," *IEEE Transactions on Electron Devices*, Sep. 2015.
- [10] S. Khandelwal, Y. S. Chauhan *et al.*, "BSIM-IMG: A Compact Model for Ultrathin-Body SOI MOSFETs With Back-Gate Control," *IEEE Transactions on Electron Devices*, vol. 59, pp. 2019–2026, 2012.
- [11] T. Elewa, F. Balestra *et al.*, "Performance and physical mechanisms in SIMOX MOS transistors operated at very low temperature," *IEEE Transactions on Electron Devices*, vol. 37, pp. 1007–1019, April 1990.

- [12] R. Trevisoli, M. de Souza *et al.*, "Junctionless nanowire transistors operation at temperatures down to 4.2 K," *Semiconductor Science and Technology*, 2016.
- [13] I. M. Hafez, G. Ghibaudo, and F. Balestra, "Assessment of interface state density in silicon MOS transistors at room, liquid nitrogen, and liquid helium temperatures," *Journal of Applied Physics*, no. 4, 1990.
- [14] A. Beckers, F. Jazaeri *et al.*, "Cryogenic characterization of 28 nm bulk CMOS technology for quantum computing," in *47th European Solid-State Device Research Conference (ESSDERC)*, Sept 2017, pp. 62–65.
- [15] A. Beckers, F. Jazaeri, and C. Enz, "Characterization and Modeling of 28 nm Bulk CMOS Technology down to 4.2 K," *IEEE Journal of the Electron Devices Society*, pp. 1–1, 2018.
- [16] A. Beckers, F. Jazaeri, and C. Enz, "Cryogenic MOS Transistor Model," *IEEE Transactions on Electron Devices*, pp. 1–9, 2018.
- [17] D. P. Foty, "Impurity ionization in MOSFETs at very low temperatures," *Cryogenics*, vol. 30, no. 12, pp. 1056 – 1063, 1990.
- [18] C. Enz, F. Chicco, and A. Pezzotta, "Nanoscale MOSFET Modeling: Part 1: The Simplified EKV Model for the Design of Low-Power Analog Circuits," *IEEE Solid-State Circuits Magazine*, vol. 9, no. 3, 2017.
- [19] A. Pezzotta, F. Jazaeri *et al.*, "A design-oriented charge-based simplified model for FDSOI MOSFETs," in *2018 Joint International EUROSOFI Workshop and International Conference on Ultimate Integration on Silicon (EUROSOFI-ULIS)*, March 2018, pp. 1–4.